Acta Crystallographica Section D
Biological Crystallography
ISSN 0907-4449

NH_3-dependent NAD^+ synthetase from *Bacillus subtilis* at 1 Å resolution

Jindrich Symersky,[a]† Yancho Devedjiev,[a]†‡ Karen Moore,[a] Christie Brouillette[a,b] and Larry DeLucas[a]*

[a]Center for Biophysical Sciences and Engineering, University of Alabama at Birmingham, Birmingham, AL 35294, USA, and [b]Department of Biochemistry, University of Alabama at Birmingham, Birmingham, AL 35294, USA

† These authors have made an equal contribution to this paper.
‡ Present address: Department of Molecular Physiology and Molecular Biophysics, University of Virginia, Charlottesville, VA 22906, USA.

Correspondence e-mail: delucas@cbse.uab.edu

Received 14 December 2001
Accepted 15 April 2002

PDB Reference: NAD^+ synthetase, 1kqp, r1kqpsf.

The final step of NAD^+ biosynthesis includes an amide transfer to nicotinic acid adenine dinucleotide (NaAD) catalyzed by NAD^+ synthetase. This enzyme was co-crystallized in microgravity with natural substrates NaAD and ATP at pH 8.5. The crystal was exposed to ammonium ions, synchrotron diffraction data were collected and the atomic model was refined anisotropically at 1 Å resolution to R = 11.63%. Both binding sites are occupied by the NAD-adenylate intermediate, pyrophosphate and two magnesium ions. The atomic resolution of the structure allows better definition of non-planar peptide groups, reveals a low mean anisotropy of protein and substrate atoms and indicates the H-atom positions of the phosphoester group of the reaction intermediate. The phosphoester group is protonated at the carbonyl O atom O7N, suggesting a carbenium-ion structure stabilized by interactions with two solvent sites presumably occupied by ammonia and a water molecule. A mechanism is proposed for the second catalytic step, which includes a nucleophilic attack by the ammonia molecule on the intermediate.

1. Introduction

NAD^+ is an essential component of many biochemical processes in living organisms. The biosynthesis of NAD^+ is pursued either *de novo* or through a pyridine nucleotide-salvage pathway (Foster & Moat, 1980; White, 1982). The two pathways merge at nicotinic acid mononucleotide, which is then adenylated to yield nicotinic acid adenine dinucleotide (NaAD). The final step of NAD^+ biosynthesis is the conversion of NaAD to NAD^+ catalyzed by NAD^+ synthetase (EC 6.3.5.1). The conversion proceeds through an NAD-adenylate intermediate, which is formed in the presence of ATP and Mg^{2+} (Preiss & Handler, 1958). The intermediate is subsequently cleaved by ammonia to yield NAD^+ and AMP (Fig. 1). The NAD^+ synthetase and/or its gene *NadE* have been identified in a number of prokaryotes, including *Escherichia coli* (Spencer & Preiss, 1967) and *Bacillus subtilis* (Nessi *et al.*, 1995), and in bacterial pathogens such as *Mycobacterium tuberculosis* (Cantoni *et al.*, 1998), *Pseudomonas aeruginosa* (Stover *et al.*, 2000) and *B. anthracis* (unpublished data). Because NAD^+ is involved in virtually all metabolic pathways, NAD^+ synthetase has been suggested as a possible target for development of a new class of antibiotics (Rizzi *et al.*, 1998). In theory, inhibitors specific for bacterial NAD^+ synthetases should decrease NAD^+ levels in pathogens, thereby inhibiting bacterial growth. The enzyme demonstrates a high sequence homology in a variety of prokaryotes and uses ammonia instead of glutamine as its source of nitrogen. Eukaryotic NAD^+ synthetases belong to the family of amidotransferases that have been shown to have an additional domain that

enables the enzyme to use glutamine as a nitrogen source (Zalkin, 1993).

The basic structural, mechanistic and functional aspects of the NAD^+ synthetase from *B. subtilis* have been extensively studied by Rizzi *et al.* (1996, 1998) and by Devedjiev *et al.* (2001). The enzyme consists of a tight homodimer ($M_r \simeq 60\,000$) with an α/β-subunit topology. The ATP-binding site is located at the classical α/β topological switch point (Rossmann *et al.*, 1975), whilst a novel NaAD-binding site was found in an adjacent cleft at the subunit interface. Stoichiometrically, there is one ATP-binding site and one NaAD-binding site per subunit. Functionality of the enzyme requires conformational changes in two surface loops including residues 82–87 and 204–225 with defined roles in substrate recognition and stabilization as well as in protection of the reaction intermediate.

Rizzi *et al.* (1998) reported the structure of NAD^+ synthetase in a complex with NAD-adenylate intermediate at 1.3 Å resolution. The protein was co-crystallized on Earth with the reaction product NAD^+ and with ATP at pH 5.2. The reaction in Fig. 1 was reversed by the low pH and the intermediate was trapped in a stable complex with the enzyme. Devedjiev *et al.* (2001) showed structural differences, at 1.9 Å resolution, in the active site of NAD^+ synthetase co-crystallized at pH 7.5 with a non-hydrolyzable analog of ATP, α,β-methyleneadenosine triphosphate. An atomic resolution structure was sought to reveal stereochemical details, anisotropic thermal motion, multiple conformations, H atoms and protonation states. Each of these features can facilitate our understanding of the detailed enzymatic mechanism (Dauter *et al.*, 1997).

The NAD-adenylate intermediate can be prepared *in situ* by the co-crystallization of NAD^+ synthetase with NaAD and ATP at pH 8.5, which is the optimal pH for activity of the enzyme from *E. coli* (Spencer & Preiss, 1967). Crystallization conditions were optimized and subsequently the microgravity environment was exploited to obtain crystals that diffracted to 1.0 Å resolution (using synchrotron radiation). Ammonium ions could be diffused into the crystals without causing significant damage. These crystals allowed data collection and refinement of the structure of NAD^+ synthetase with the NAD-adenylate intermediate at 1 Å resolution. The atomic resolution features are discussed and implications shown for the enzyme mechanism.

2. Experimental

2.1. Crystallization and data collection

NAD^+ synthetase was expressed and purified as described by Devedjiev *et al.* (2001). Crystals of the enzyme were grown in microgravity during the US Space Shuttle Mission STS-95 using a microseeding technique adapted for microgravity experiments. The crystals were grown by vapor diffusion using the Commercial Vapor Diffusion Apparatus (CVDA; DeLucas *et al.*, 1994). First, seed crystals of NAD^+ synthetase with NaAD and 2.5 m*M* ATP were grown on Earth at pH 5.2 using the procedure reported by Devedjiev *et al.* (2001). Crushed seed crystals were then placed in a solution of 25%(*v*/*v*) PEG 400, 50 m*M* Tris pH 8.5, 50 m*M* magnesium chloride, 5 m*M* NaAD and 2.5 m*M* ATP (buffer *A*) and serial dilutions were made. Prior to the Shuttle launch, the CVDA hardware was loaded with protein droplets made up of 1:1 mixtures of 15 mg ml^{-1} NAD^+ synthetase solution and the various seed solutions. After orbit was attained, the experiments were activated and the protein droplets were equilibrated against 25%(*v*/*v*) PEG 400 solution for 9 d. The hardware was returned to Earth and the crystals were harvested and stored in buffer *A*.

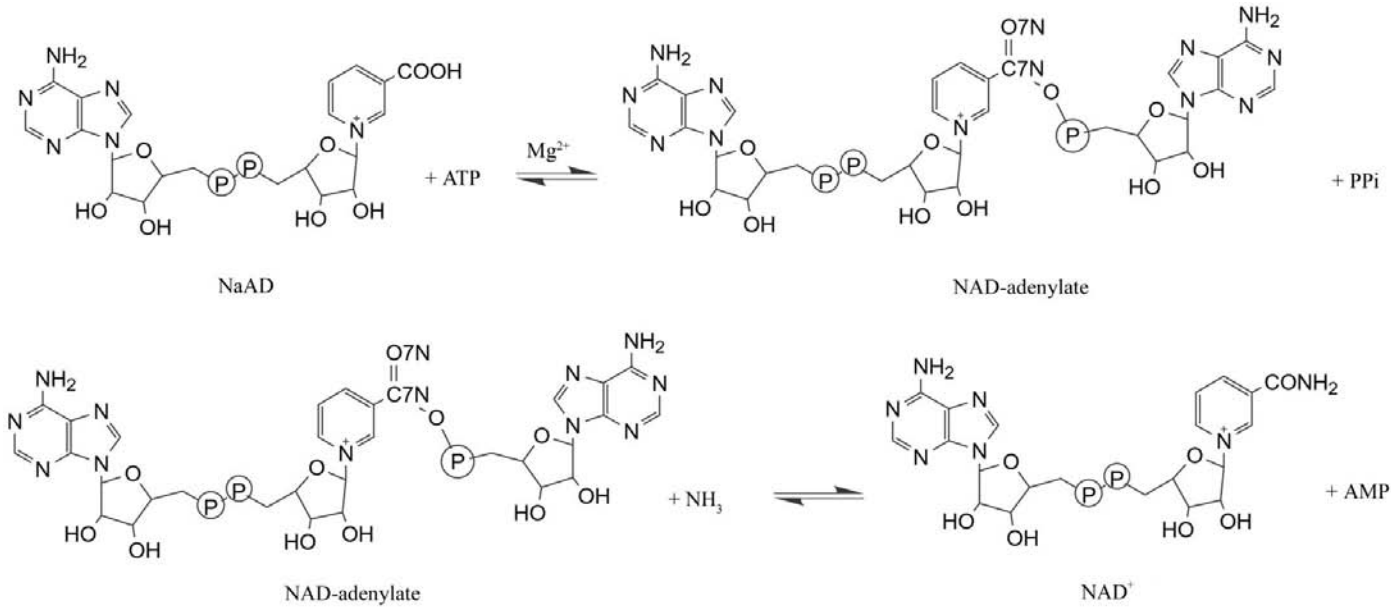

Figure 1
A scheme of the reaction catalyzed by NAD^+ synthetase.

Table 1
The crystal and data-collection statistics for NAD^+ synthetase.

Values in parentheses refer to the last resolution shell.

Unit-cell parameters (Å, °)	a = 52.28, b = 84.79, c = 59.64, α = 90, β = 110.5, γ = 90
Space group	$P2_1$
Matthews coefficient (Å^3 Da^{-1})	1.97
Solvent content (%)	36.0
Resolution range (Å)	30.0–1.03 (1.10–1.03)
No. of measured reflections	790765
No. of unique reflections	231200
Completeness (%)	90.0 (75.0)
R_{sym}† (%)	4.8 (38.1)
$I/\sigma(I)$	32.8 (2.4)
No. of reflections with $I > 4\sigma(I)$	170606

† $R_{sym} = \sum |I_i - \langle I_i \rangle| / \sum I_i$, where $\langle I_i \rangle$ is the average of the i intensity measurements.

Table 2
Refinement statistics for NAD^+ synthetase complexed with NAD-adenylate intermediate.

$R = \sum \big||F_o| - |F_c|\big| / \sum |F_o|$, where $|F_o|$ and $|F_c|$ are the observed and calculated structure-factor amplitudes, respectively. The target bond lengths and angles are those of Engh & Huber (1991). $\langle B \rangle$ is a mean isotropic equivalent temperature factor.

Resolution range (Å)	10.0–1.03
No. of reflections in refinement	205215
No. of parameters	47101
No. of restraints	57173
No. of non-H atoms (excluding waters)	4518
No. of full/partial water sites	543/171
R factor (%)	11.63
R_{free} (%)	14.72
Goodness of fit	1.348
$\langle B \rangle$ for all protein atoms (Å^2)	14.51
$\langle B \rangle$ for main-chain atoms (Å^2)	10.41
$\langle B \rangle$ for side-chain atoms (Å^2)	16.83
$\langle B \rangle$ for NAD-ad, PP_i and Mg^{2+} (Å^2)	13.93
$\langle B \rangle$ for water atoms (Å^2)	25.14
$\langle B \rangle$ for ethylene glycol (Å^2)	25.36
RMS deviations from target values	
Bond lengths (Å)	0.015
Bond angles (Å)	0.031
Bond angles (°)	2.2
Chiral volumes (Å^3)	0.083

The diffraction data were collected on beamline X11 at EMBL-Hamburg c/o DESY, Germany. The wavelength of the incident radiation was 0.905 Å and diffracted X-rays were detected using a MAR 345 image-plate scanner. Prior to flash-freezing at 120 K in a stream of nitrogen, the crystal (0.2 × 0.1 × 0.1 mm) was conditioned for several seconds in a solution composed of buffer *A* with the addition of 20%(*v*/*v*) ethylene glycol and 25 m*M* NH_4Cl. In the first pass, a total of 120 diffraction images were collected within the resolution shell 30–1.7 Å with an oscillation range of 1.5° per image. In the second pass, 280 images with an oscillation range of 0.65° were collected to 1 Å resolution. The diffraction images were processed with *DENZO* and *SCALEPACK* (Otwinowski & Minor, 1997). Data from the second pass within the resolution shell 2.25–1.03 Å were merged with the complete data from the first pass. The statistics of the synchrotron data collection are shown in Table 1.

Control crystals were also grown on Earth at pH 8.5 under similar conditions by the vapor-diffusion technique in micro-seeded hanging drops. The control crystals diffracted to 1.95 Å using a rotating-anode X-ray source. This resolution is comparable to the in-house data collected previously on isomorphous NAD^+ synthetase structures at pH 5.2 and 7.5 (Devedjiev *et al.*, 2001). The space-grown crystals, however, diffracted to 1.47 Å using the same rotating-anode X-ray source. Apparently, it is the microgravity rather than the pH that has enhanced the resolution. The effects of microgravity and further comparison with Earth-grown structures will be reported in detail elsewhere (in preparation).

2.2. Refinement

Refinement was initiated using an isomorphous NAD^+ synthetase structure (PDB code 1ee1; Devedjiev *et al.*, 2001). The active-site loops 82–87 and 204–225 were removed and the starting model included no ligands or solvent molecules. A subset of 5% of randomly selected reflections was used for cross-validation analysis (Brünger, 1992). At the first stage, the model was refined in *CNS* (Brünger *et al.*, 1998) at 2 Å resolution. After a rigid-body minimization, the R factor was 36% and R_{free} was 36.3%. A cycle of simulated annealing followed by positional refinement improved the R factors to 30.6 and 34%, respectively. Several more rounds of positional refinement combined with manual model building in *O* (Jones *et al.*, 1993) lowered the R factor to 18.5% and R_{free} to 22.2%. The model building included addition of missing loops in both subunits, adjustment of side chains throughout the model, addition of NaAD, AMP, PP_i, Mg^{2+} and well defined water molecules after a bulk-solvent correction. Only single conformations of side chains were considered at this stage. $2F_o - F_c$ and $F_o - F_c$ electron-density maps were calculated in *CNS* and displayed in *O*. Refinement of isotropic displacement parameters of non-H atoms decreased the R factor to 16.5% and R_{free} to 20.3% and it became increasingly clear that the NAD-adenylate intermediate and PP_i occupy the corresponding binding sites in both subunits.

The model was further refined using *SHELX*97 (Sheldrick, 1997; Sheldrick & Schneider, 1997) at 1 Å resolution. Program defaults were used for all distance, planarity and chiral restraints. The program does not support torsion-angle restraints. Protein target values were taken from Engh & Huber (1991) and those for the NAD-adenylate intermediate were calculated using the coordinates of the NAD^+ small-molecule crystal structure (entry CEVYEH01) from the Cambridge Structural Database (Allen & Kennard, 1991). Average bond lengths and angles of corresponding entries from the database were the target values for ethylene glycol. No restraints were used for PP_i and Mg^{2+}. The phosphoester group (reaction center) including the carbonyl C7N═O7N, ester O atom and one C atom of the nicotine ring (Fig. 1) was also unrestrained. Initially, H atoms were not included. After 27 cycles of conjugate-gradient least-squares minimization of positional and isotropic displacement parameters, the R factor for all data was 17.5% and R_{free} was 19.6%. A number of

double or triple conformations of side chains became apparent in the $2F_o - F_c$ and $F_o - F_c$ electron-density maps calculated in *CNS* with a bulk-solvent correction. Frequently, a residual density at 2–3σ consistent with the expected position of an H atom was observed at the protein or at the substrate. For well ordered (and usually buried) side chains of Asn, Gln and His residues, it was possible to correctly assign protonated N atoms. For most side chains of this type, however, the protonation was ambiguous and interactions with neighboring atoms were considered for final positioning. After every ninth cycle, water molecules with electron density lower than 1σ in the $2F_o - F_c$ map and with B factors above 45 Å^2 were excluded. Water molecules with electron density above 1σ and B factors higher than 45 Å^2 were included and their occupancy was set to 0.5. Peaks in the $F_o - F_c$ map with electron density of 0.5 e Å^{-3} or higher and within 2.0–4.0 Å of non-H atoms were included as new water molecules with full occupancy. The multiple conformations of side chains were added to the model with restrained occupancies (sum = 1).

In the final stage of the refinement in *SHELX*97, all but the carboxylic H atoms were calculated for the standard amino-acid residues and one restrained parameter per H atom was allowed for the isotropic thermal vibration (atomic displacement). Positions of the H atoms were restrained using the 'riding model'. Six parameters describing the anisotropy of thermal vibrations were assigned to each non-H atom. The atomic displacement parameters for both H and non-H atoms were restrained using the default program values. A bulk-solvent correction, as implemented in *SHELX*97, was also activated in the refinement. The atomic positional and displacement parameters were refined simultaneously with free variables that represented restrained occupancies of the multiple conformations. Another 27 refinement cycles were run with two sessions of manual model building, which included editing solvent molecules and multiple conformations. During the last nine cycles, selected H atoms were added to the NAD-adenylate intermediate and the resolution of the data was limited to the 10.0–1.0 Å resolution shell owing to the poor analysis of variance for data between infinity and 10 Å. As the reflection-to-parameter ratio was only about 4, all restraints were kept in the final cycles. The R factor converged at 11.63% for all data and the $R_{\rm free}$ at 14.72%. The refinement statistics are summarized in Table 2.

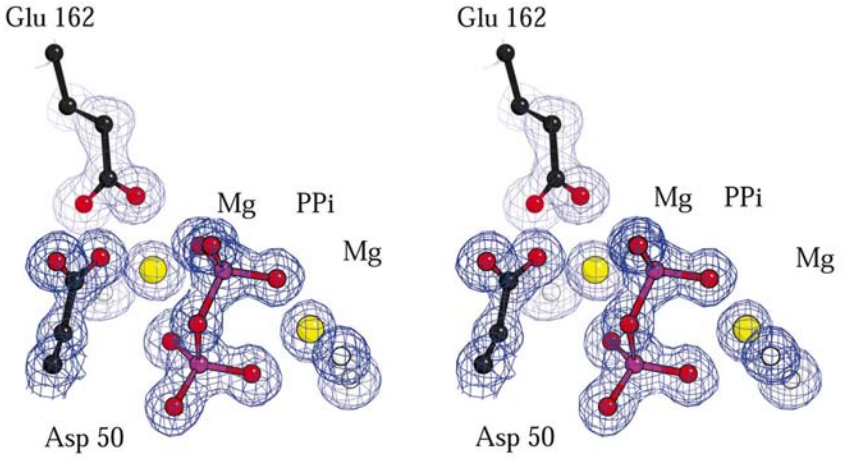

Figure 2
A sample of the $2F_o - F_c$ electron-density map contured at the 3σ level showing the pyrophosphate and magnesium ions in subunit A.

3. Results and discussion

3.1. An overview of the refined structure

The final model consists of two complete sequences of 542 amino-acid residues, two molecules of the NAD-adenylate intermediate, two pyrophosphates, five magnesium ions, ten ethylene glycol molecules and 714 water sites. The two main chains assume single well ordered conformations without breaks in the $2F_o - F_c$ electron-density map at the 1.5σ level. The Ramachandran plot (Ramachandran *et al.*, 1963) has 89% of the residues in the most favored regions and 11% in allowed regions. The side chains of 18 amino-acid residues have been found in double or triple conformations and another 18 polar residues exposed at the surface have disordered side chains. For most regions of the model, the electron density of individual atoms is visible at the 4σ level. The pyrophosphates and magnesium ions, refined without restraints, have continuous electron density at the 3σ level (Fig. 2) and individual atoms are seen even at 6σ. Ethylene glycol molecules bound at the protein surface have continuous electron density at 1.5σ, but relatively higher temperature factors. There are 543 ordered water sites with full occupancies, which represents the calculated solvent content of approximately 25% (*cf.* Table 1). The other 171 water sites have been refined with half occupancies. All solvent atoms are seen at the 1σ level. Approximately one third of the protein H atoms and several H atoms of the substrates (Figs. 3*a* and 3*b*) could be identified in the $F_o - F_c$ electron-density map before they were included in the model. A number of active-site residues revealed most H atoms in the expected positions, as shown for Tyr*A*144 in Fig. 3(*c*). Solvent molecules, however, revealed H-atom positions only exceptionally and it was not possible to distinguish ammonium ions from water molecules. The final model with H atoms has a number of H—H contacts shorter than 2.2 Å, which is not unusual in atomic resolution structures deposited in the Protein Data Bank. The model scored high *via* analysis by *PROCHECK* (Laskowski *et al.*, 1993), although lower resolution structures often score better owing to tighter geometry restraints. The deviations from target geometry values are similar to those reported from other atomic resolution structures (Table 2). An overall coordinate error of 0.05 Å has been estimated using a

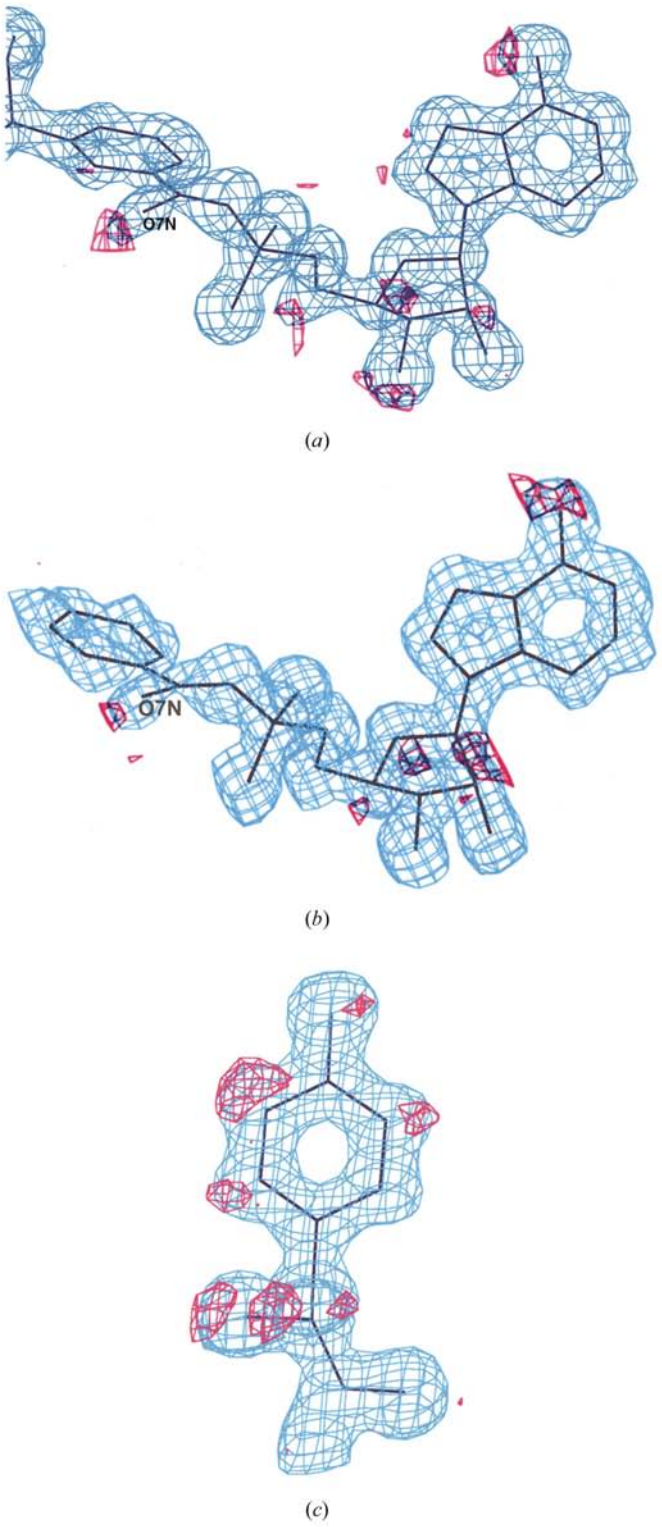

Figure 3
H-atom positions (red) as indicated by $F_o - F_c$ electron-density map before including H atoms in the model. (*a*) The NAD-adenylate intermediate in subunit *A*. Only the relevant part is shown, including the AMP moiety and the nicotine ring. The $F_o - F_c$ map is contoured at 2.5σ; the $2F_o - F_c$ map (blue) is shown at 1.5σ. (*b*) The NAD-adenylate intermediate in subunit *B*. The $F_o - F_c$ map is contoured at 1.5σ; the $2F_o - F_c$ map (blue) is shown at 1σ. (*c*) An example of active-site residue Tyr*A*144 with all but one H atom apparent in the $F_o - F_c$ map contoured at 2.5σ. The $2F_o - F_c$ map (blue) is shown at 1.5σ.

Luzzati plot (Luzzati, 1952). In addition, a mean estimated standard deviation for protein and substrate atoms has been calculated to be 0.031 Å, based on one blocked full-matrix refinement cycle in *SHELX*97.

3.2. Planarity of peptide groups

Although the overall standard deviation of the ω torsion angle (peptide planarity) is 5.6°, which is similar to the values found in other well determined structures, there are 31 peptide groups in this structure with deviations from planarity between 11 and 17°. Nevertheless, the corresponding amino-acid residues are well ordered, with good electron density and, in addition, their main-chain atoms were restrained in a similar fashion to other peptides during the refinement. Retrospectively, these 31 peptide groups were almost planar, with deviations of less than 5° after refinement in *CNS* (see §2.2). Significantly non-planar peptide groups have also been found in other high-resolution structures (*e.g.* MacArthur & Thornton, 1996; Wilson *et al.*, 1998; Sandalova *et al.*, 1999; Addlagatta *et al.*, 2001). In the last example, the structure was refined at even higher resolution with no restraints for the main chain. These findings present growing evidence that the peptide group, although postulated as planar (Pauling, 1945), may assume surprisingly twisted conformations in protein structures. MacArthur & Thornton (1996) have shown that proteins with high α-helical content have considerably lower deviations from planarity of the peptide groups. The hydrogen bonding of the α-helix enhances the double-bond character of the peptide group, thus making it more planar. In a sample of high-resolution structures, Sandalova *et al.* (1999) did not find a correlation between residue type and non-planarity of the peptide group. As we observed in this structure, the non-planar peptide groups are only found in turns that precede or follow more regular motifs of the secondary structure (helices, strands) or in coiled regions.

3.3. Analysis of anisotropic displacement

The anisotropic refinement of non-H atoms improved the *R* factor and $R_{\rm free}$ by 4.1 and 3.3%, respectively. After a least-squares fit, RMS deviations between the isotropic and anisotropic sets of atomic coordinates were 0.03 Å for C^{α} atoms and

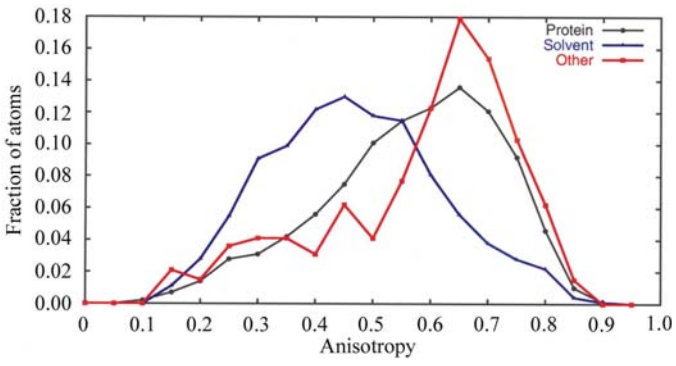

Figure 4
Distribution of anisotropy by atom class for the NAD^+ synthetase crystal structure refined at 1 Å resolution.

0.29 Å for all non-H atoms, excluding the solvent atoms. A distribution of anisotropy is shown in Fig. 4. A perfectly isotropic atom has an anisotropy equal to 1.0. As the anisotropy decreases to 0.0, it describes an increasingly elongated ellipsoid or a disk. The mean anisotropy of protein atoms is 0.592, with a standard deviation of 0.152. The values are similar for ligand atoms, whereas the solvent atoms have a mean anisotropy of 0.493 with a standard deviation of 0.148. Distributions for protein and ligand atoms in Fig. 4 show considerably less anisotropy than expected. Merritt (1999) analyzed a set of atomic resolution structures from the Protein Data Bank and concluded that a typical distribution of anisotropy was symmetrical with a mean of 0.45 and a standard deviation of 0.15. For the structures that deviate significantly from the typical distribution, Merritt suggested the revision of restraints applied during the anisotropic refinement. In this study, the ISOR restraint, which approximates isotropic behavior, has been used only for solvent atoms. Thus, the only restraints that could possibly enforce more isotropy to protein and ligand atoms were SIMU and DELU. SIMU restrains anisotropic components of neighboring atoms to be similar. DELU restrains anisotropic components of bonded atoms to be equal in the direction of the bond. We have re-refined the structure starting from the original isotropic model without applying SIMU and DELU restraints in 15 cycles of conjugate-gradient least-squares minimization in *SHELX*97. A DAMP factor of 0.1 was necessary for stability. Although the refinement produced an increased number of outliers with extreme anisotropy, the distribution of anisotropy was essentially the same, with a mean of 0.584 and a standard deviation of 0.156 for protein atoms. The *R* factor was lowered to 11.50%; however, the $R_{\rm free}$ increased to 14.77%. We therefore conclude that this structure has inherently less atomic displacement than the average observed previously. In fact, there is at least one well refined structure with a similar distribution of anisotropy (PDB code 1gci). As a globular and relatively large protein assembly, NAD^+ synthetase increases atomic displacement with distance from the center of mass (not shown). The largest displacement (and thereby the lowest mean anisotropy) is consistently observed in exposed loops and side chains. Smaller proteins and those with more complex tertiary structures may naturally have lower mean anisotropy values than typical globular proteins. However, an extensive analysis using a large sample of structures is beyond the scope of this paper.

3.4. Comparison with structures at pH 5.2

The present structure is isomorphous with the NAD^+ synthetase structure determined by Rizzi *et al.* (1998) at pH 5.2. The unit-cell volumes agree within 2% and the two sets of C^α atoms have an RMS deviation of 0.36 Å. Average temperature factors are somewhat lower (by 1.5 $Å^2$) in the higher resolution structure. The superimposed models show only subtle differences in positions of ordered side chains and, in some regions, rigid-body shifts of approximately 0.5 Å. The substrates, ions and water molecules in the active site are also in identical or similar positions. While Rizzi *et al.* (1998) reported seven side chains in double conformations, we found 14 in double conformations and four in triple conformations. Five such residues are identical between the two structures. Generally, all of the side chains with multiple conformations have few or no contacts with neighboring residues or with the symmetry-related molecules. Only two such residues are found in hydrophobic pockets and the others reside at the surface. None of the residues with multiple side-chain conformations are part of the active site. A new magnesium site was found with the typical octahedral coordination interacting with five water molecules and the carboxyl group of Asp*B*124. This magnesium ion is distant, however, from both active sites and apparently not involved in catalysis.

Remarkably, the two high-resolution structures crystallized at different pH values and using different substrates (see third paragraph of §1) have few differences and essentially the same active sites with the reaction intermediate bound. In order to protect the reaction intermediate, the majority of the active site is covered by two stabilized loops described previously (Devedjiev *et al.*, 2001). Apparently, even a large difference in pH does not affect the closed structural arrangement. Differences in the active site with bound α,β-methylene-adenosine triphosphate observed by Devedjiev *et al.* (2001) were caused primarily by the absence of NaAD rather than by the higher pH. It is known, however, that both the first and second steps of the enzyme reaction are pH-dependent. Devedjiev *et al.* (2001) also co-crystallized NAD^+ synthetase with NaAD and ATP at pH 5.2 and found intact substrates in the active site and the Mg(I) site unoccupied (PDB code 1ee1). The reaction intermediate was eventually observed after soaking these crystals in artificial mother liquor at pH 6.8 (unpublished data). It shows that the reaction center must be accessible to the solvent molecules and ions even in the closed state. The access is most probably facilitated by the solvent 'channel' described by Rizzi *et al.* (1998). In the present atomic resolution structure crystallized at pH 8.5, the electron density of the buried phosphates and carboxyl groups does not suggest any protonation. However, at pH 5.2, one or more of the negatively charged groups may be protonated through the solvent channel. The first reaction step may then be blocked by protonation of the α- or β-phosphate O atoms of ATP. This may prevent magnesium from assuming the position at Mg(I) which is responsible for weakening the bond between the α- and β-phosphate. Mechanistic aspects of the second reaction step and the role of pH are discussed in the next section.

3.5. The reaction intermediate

As originally proposed by Preiss & Handler (1958), the NAD-adenylate intermediate is formed in the first reaction step before the nucleophilic attack by an ammonia molecule (Fig. 1). This intermediate is analogous to that proposed for the activation of acetate (Berg, 1956) and amino-acid carboxyl groups (Kamin & Handler, 1957), which do not have the nicotine ring. We have refined the two NAD-adenylate molecules in essentially the same conformation as Rizzi *et al.*

(1998) with similar patterns of interactions with the protein residues, ions and solvent molecules in the active site. The reaction center at C7N was refined without restraints with bond lengths and angles comparable to those reported by Rizzi *et al.* (1998), except for the shorter bond length between C7N and O2P (1.19 Å in subunit *A* and 1.25 Å in subunit *B*). The individual atoms of the ADP and AMP moieties have spherical electron density in the $2F_o - F_c$ map at the 4σ level. In subunit *A*, the ribose atoms of the nicotinosyl moiety remain visible at the 4σ level, while the nicotine ring and the carbonyl require the 2σ level. In subunit *B*, the entire nicotinosyl moiety is displayed at 1.5σ and the atoms are refined with higher temperature factors. Thus, the intermediate is better defined in subunit *A*.

Before adding any H atoms to the intermediate, several peaks were observed in the $F_o - F_c$ electron-density map at the ribose and at the adenine base in positions where H atoms could be anticipated (Figs. 3*a* and 3*b*). Moreover, the significant residual electron density in the same relative position ~0.8 Å from the atom O7N in both molecules was persistent even after anisotropic refinement and addition of H atoms to the ribose and adenine ring. The residual peak at O7N was apparent at the 3σ level in subunit *A* and somewhat lower in subunit *B* at 1.5σ. Also, a large anisotropy of the atom O7N was observed in both molecules. An unrestrained H atom was included at O7N in both molecules during the last refinement cycles. As a result, the final $F_o - F_c$ map at the 1σ level does not reveal any residuals at O7N and the H atoms have been refined with good bond lengths and angles (0.83 Å and 105° in subunit *A*; 0.82 Å and 111° in subunit *B*). In order to minimize the possibility that the electron-density peaks corresponding to the H-atom position at O7N could come from a few mismeasured intensities, we have re-refined the model without the H atoms at O7N in nine anisotropic cycles using only the high-resolution data in the resolution range 6–1 Å and, in addition, we excluded 33 intensities with the largest differences between observed and calculated normalized amplitudes. The same purged data was used to calculate a new difference map. The peaks reappeared in the same positions and at the same σ levels. The position of the H atom at O7N suggests that the intermediate may exist as a carbenium ion, rather than a conventional phosphoester.

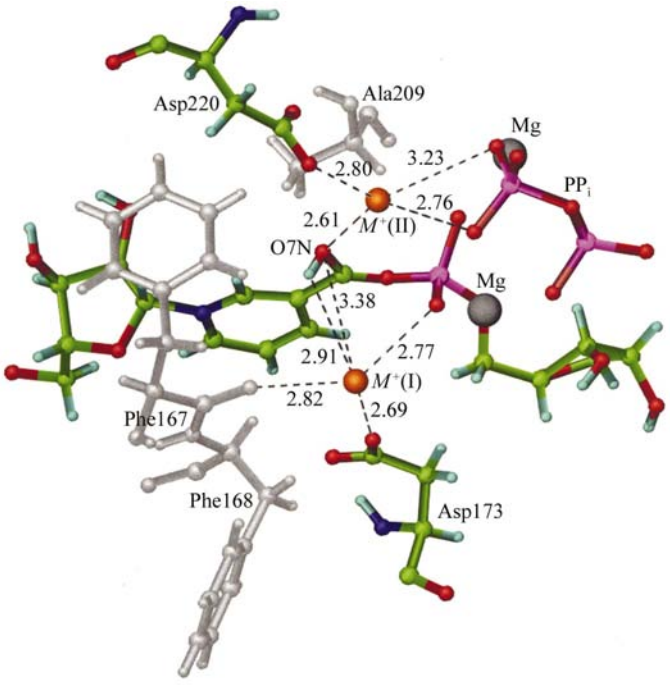

Figure 5
Spatial relationship between the intermediate protonated at O7N and cation-binding sites M^+(I) and M^+(II). Distances are shown in Å for subunit *A*. C atoms are in green, N atoms in blue, O atoms in red, P atoms in magenta and H atoms in cyan. Hydrophobic residues are all in gray, magnesium ions in black and the monovalent cation-binding sites M^+(I) and M^+(II) are shown as golden spheres. Rendered using *RIBBONS* (Carson, 1997).

Carbenium ions, although generally unstable, have been determined in small-molecule systems using ^{1}H and ^{13}C NMR techniques at temperatures between 195 and 153 K (Olah, 2001). In the NAD$^+$ synthetase structure there are no protein residues that would directly interact with the reaction center and stabilize the carbenium-ion intermediate. However, the enzyme provides convenient solvent sites within hydrogen-bonding distance of the carbonyl group C7N═O7N of the intermediate (Fig. 5). These sites coincide with monovalent cation-binding sites denoted M^+(I) and M^+(II) determined by Rizzi *et al.* (1998). In addition, as shown by Devedjiev *et al.* (2001), the bound ATP and the nicotinosyl part of NaAD are totally buried. Thus, the isolation from the bulk solvent and the cryogenic temperature of the data collection may also be important stabilizing factors for the intermediate. The low temperature and short exposure to ammonium ions may account for the fact that the reaction does not proceed towards NAD$^+$ and AMP.

A well defined water site has been refined at M^+(I), 3.12 Å from the atom C7N of the intermediate in subunit *A* and 2.76 Å in subunit *B*. Similarly, there is a water site at M^+(II), 2.61 Å from O7N in subunit *A* and 2.86 Å in subunit *B*. Both protein and substrate contribute to formation of the cation-binding sites (Fig. 5). M^+(I) is coordinated to the carboxyl O atom of Asp173, the carbonyl O atom of Phe167, the α-phosphate O atom of the intermediate and possibly the carboxyl O atom of Glu162 (although this carboxyl is better positioned for coordination to Mg^{2+}). A longer hydrogen-bond contact is observed between M^+(I) and O7N of the intermediate. This may also be a stabilizing contact for the protonated reaction center. M^+(II) has a number of contacts with pyrophosphate O atoms and with α-phosphate O atoms of the intermediate. In addition, the carboxyl group of Asp220 and the O7N atom of the intermediate are also coordinated to M^+(II) as shown in Fig. 5.

The site M^+(I) is especially well positioned for the nucleophilic attack on C7N. Rizzi *et al.* (1998) proposed that this site is occupied by an ammonium ion and showed how the ammonium ion is transported from the protein surface through a solvent channel to the buried site M^+(I). The final reaction step requires a neutral ammonia molecule and a defined electrophilic center at C7N. Rizzi *et al.* (1998)

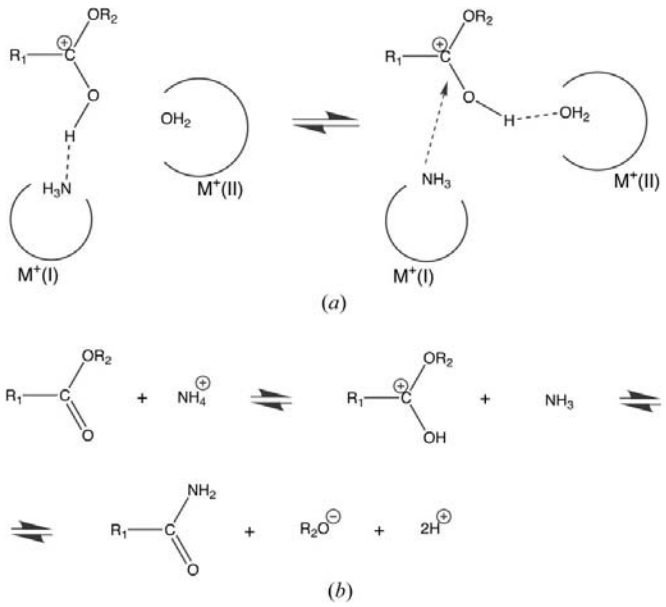

Figure 6
(*a*) Stabilization of the protonated intermediate by the hydrogen bond with ammonia positioned in the cation-binding site M^+(I) and a hypothetical hydrogen bond with water molecule in the cation-binding site M^+(II) releasing the ammonia molecule for nucleophilic attack. (*b*) Reaction scheme for the second catalytic step of NAD^+ synthetase. The NAD-adenylate intermediate reacts with ammonia to form NAD^+ and AMP and two protons are released. R_1 represents the ADP-nicotinosyl moiety and R_2 represents the AMP moiety.

suggested that the ammonium ion at M^+(I) is deprotonated by Asp173 and that the site M^+(II) may be occupied by a potassium ion, as KCl was shown to enhance NAD^+ production (Spencer & Preiss, 1967). The K^+ ion has an electron-withdrawing effect on the carbonyl group of the intermediate and thus supports formation of the electrophilic center at C7N. However, at 1 Å resolution and with ammonium ions introduced we do not see any protonation of Asp173 or any other carboxyl group in the active site. Instead, we have a strong indication for the protonated intermediate at O7N. Furthermore, Spencer & Preiss (1967) have shown for the *E. coli* enzyme that KCl is not necessary for the enzyme activity and our assays show the same for the *B. subtilis* enzyme (unpublished data). Based on our observation of the protonated intermediate, we propose that the protonation of the carbonyl group C7N═O7N precedes the final reaction step and the proton transfer originates from the ammonium ion at M^+(I) (Fig. 5). At this stage, the second site M^+(II) is probably occupied by a water molecule which may eventually help to release the free ammonia molecule (and trigger the nucleophilic attack) by creating a new hydrogen bond O7N—H7N···O (Figs. 5 and 6*a*). This would require a torsion rotation of H7N around the bond C7N—O7N of approximately 120°. In the refined structure, we observe the H atom H7N in a different position, still engaged in a hydrogen-bond contact with what is presumably an ammonia molecule (Fig. 5). This may also explain why the reaction does not proceed by nucleophilic attack in the crystal structure. The second step of the enzyme reaction can be formally described by the scheme in Fig. 6(*b*). Two protons are released from the reaction complex and trapped as H_3O^+ ions in the cation-binding sites M^+(I) and M^+(II). The active site opens through the loops 82–87 and 204–225 as soon as NAD^+ and AMP are formed. The reaction products are released and the cation-binding sites neutralized from the bulk solvent. At the low pH, however, the cation-binding sites will remain occupied by H_3O^+ ions, which will block or reverse the reaction. This mechanism is consistent with the experimental information accumulated so far.

4. Conclusions

The atomic resolution structure of NAD^+ synthetase has revealed a number of non-planar peptide groups in the main chain, low anisotropy of protein and substrate atoms, a pH-independent structure of the active site with bound intermediate and a carbenium-ion character of the reaction intermediate. While the non-planar peptide groups and lower anisotropy have already been observed in other crystal structures, the carbenium-ion intermediate is a novel finding which provides important insights into the possible mechanism of catalysis of the enzyme. The refined structure also shows that 1 Å resolution only just begins to allow identification of H-atom positions and that ultrahigh resolution studies may be necessary to obtain a full mechanistic picture of the enzymatic reaction.

The microgravity crystallization experiments were conducted in collaboration with NASA and supported by NASA Cooperative Agreement NCC8-126. This work was also supported, in part, by the Defense Advanced Research Proposal Agency. We are grateful to all referees for their constructive suggestions.

References

Addlagatta, A., Krzywda, S., Czapinska, H., Otlewski, J. & Jaskolski, M. (2001). *Acta Cryst.* D**57**, 649–663.
Allen, F. H. & Kennard, O. (1991). *Chem. Des. Autom. News*, **8**, 31–37.
Berg, P. (1956). *J. Biol. Chem.* **222**, 991–1013.
Brünger, A. T. (1992). *Nature (London)*, **355**, 472–475.
Brünger, A. T., Adams, P. D., Clore, G. M., DeLano, W. L., Gros, P., Grosse-Kunstleve, R. W., Jiang, J.-S., Kuszewski, J., Nilges, M., Pannu, N. S., Read, R. J., Rice, L. M., Simonson, T. & Warren, G. (1998). *Acta Cryst.* D**54**, 905–921.
Cantoni, R., Branzoni, M., Labo, M., Rizzi, M. & Riccardi, G. (1998). *J. Bacteriol.* **180**, 3218–3221.
Carson, M. (1997). *Methods Enzymol.* **277**, 493–505.
Dauter, Z., Wilson, K., Sieker, L. C., Meyer, J. & Moulis, J.-M. (1997). *Biochemistry*, **36**, 16065–16073.
DeLucas, L. J. *et al.* (1994). *J. Cryst. Growth*, **135**, 183–195.
Devedjiev, Y., Symersky, J., Singh, R., Jedrzejas, M., Brouillette, C., Brouillette, W., Muccio, D., Chattopadhyay, D. & DeLucas, L. (2001). *Acta Cryst.* D**57**, 806–812.
Engh, R. A. & Huber, R. (1991). *Acta Cryst.* A**47**, 392–400.
Foster, J. W. & Moat, A. G. (1980). *Microbiol. Rev.* **44**, 83–105.
Jones, T. A., Bergdoll, M. & Kjeldgaard, M. (1993). *Crystallographic Computing and Modeling Methods in Molecular Design.* New York: Springer.

Kamin, H. & Handler, P. (1957). *Annu. Rev. Biochem.* **26**, 419–490.
Laskowski, R. A., MacArthur, M. W., Moss, D. S. & Thornton, J. M. (1993). *J. Appl. Cryst.* **26**, 283–291.
Luzzati, V. (1952). *Acta Cryst.* **5**, 802–810.
MacArthur, M. W. & Thornton, J. M. (1996). *J. Mol. Biol.* **264**, 1180–1195.
Merritt, E. A. (1999). *Acta Cryst.* D**55**, 1109–1117.
Nessi, C., Albertini, A. M., Speranza, M. L. & Galizzi, A. (1995). *J. Biol. Chem.* **270**, 6181–6185.
Olah, G. A. (2001). *J. Org. Chem.* **66**, 5943–5957.
Otwinowski, Z. & Minor, W. (1997). *Methods Enzymol.* **276**, 307–326.
Pauling, L. (1945). *The Nature of the Chemical Bond*, p. 207. Ithaca, NY: Cornell Universities Press.
Preiss, J. & Handler, P. (1958). *J. Biol. Chem.* **233**, 493–500.
Ramachandran, G. N., Ramakrishnan, C. & Sasisekharan, V. (1963). *J. Mol. Biol.* **7**, 95–99.
Rizzi, M., Bolognesi, M. & Coda, A. (1998). *Structure*, **6**, 1129–1140.
Rizzi, M., Nessi, C., Mattevi, A., Coda, A., Bolognesi, M. & Galizzi, A. (1996). *EMBO J.* **15**, 5125–5134.
Rossmann, M. G., Liljas, A., Branden, C. I. & Banaszak, L. J. (1975). *The Enzymes*, edited by P. D. Boyer, pp. 61–102. New York: Academic Press.
Sandalova, T., Schneider, G., Kack, H. & Lindqvist, Y. (1999). *Acta Cryst.* D**55**, 610–624.
Sheldrick, G. M. (1997). *The SHELX*97 *Manual*. University of Göttingen, Germany.
Sheldrick, G. M. & Schneider, T. R. (1997). *Methods Enzymol.* **277**, 319–343.
Spencer, R. L. & Preiss, J. (1967). *J. Biol. Chem.* **242**, 385–392.
Stover, C. K. *et al.* (2000). *Nature (London)*, **406**, 959–964.
White, H. B. (1982). *The Pyridine Nucleotide Coenzymes*, edited by J. Everse, B. M. Anderson & K. S. You, pp. 1–17. New York: Academic Press.
Wilson, K. S., Butterworth, S., Dauter, Z., Lamzin, V. S., Walsh, M., Wodak, S., Pontius, J., Richelle, J., Vaguine, A., Sander, C., Hooft, R. W. W., Vriend, G., Thornton, J. M., Laskowski, R. A. & MacArthur, M. W. (1998). *J. Mol. Biol.* **276**, 417–463.
Zalkin, H. (1993). *Adv. Enzymol. Relat. Areas Mol. Biol.* **66**, 203–309.